Journal of Solid State Chemistry 184 (2011) 1312–1317

Contents lists available at ScienceDirect

Journal of Solid State Chemistry

journal homepage: www.elsevier.com/locate/jssc

Role of $SrMoO_4$ in Sr_2MgMoO_6 synthesis

S. Vasala, H. Yamauchi, M. Karppinen *

Laboratory of Inorganic Chemistry, Department of Chemistry, School of Chemical Technology, Aalto University, P.O. Box 16100, FI-00076 Aalto, Finland

ARTICLE INFO

Article history:
Received 18 February 2011
Received in revised form
24 March 2011
Accepted 27 March 2011
Available online 2 April 2011

Keywords:
Double-perovskite oxide
Solid oxide fuel cell
Anode
Solid-state synthesis

ABSTRACT

Here we investigate the elemental and phase compositions during the solid-state synthesis of the promising SOFC-anode material, Sr_2MgMoO_6, and demonstrate that molybdenum does not notably evaporate under the normal synthesis conditions with temperatures up to 1200 °C due to the formation of $SrMoO_4$ as an intermediate product at low temperatures, below 600 °C. However, partial decomposition of the Sr_2MgMoO_6 phase becomes evident at the higher temperatures (~1500 °C). The effect of $SrMoO_4$ on the electrical conductivity of Sr_2MgMoO_6 is evaluated by preparing a series of Sr_2MgMoO_6 samples with different amounts of additional $SrMoO_4$. Under the reducing operation conditions of an SOFC anode the insulating $SrMoO_4$ phase is apparently reduced to the highly conductive $SrMoO_3$ phase. Percolation takes place with 20–30 wt% of $SrMoO_4$ in a Sr_2MgMoO_6 matrix, with a notable increase in electrical conductivity after reduction. Conductivity values of 14, 60 and 160 S/cm are determined at 800 °C in 5% H_2/Ar for the Sr_2MgMoO_6 samples with 30, 40 and 50 wt% of added $SrMoO_4$, respectively.

1. Introduction

Fuel cells are able to directly convert the chemical energy of a fuel to electrical energy. Among such devices solid oxide fuel cells (SOFCs) are considered most promising for relatively large-scale applications, e.g. power plants and auxiliary power units for vehicles [1–3]. One of the greatest advantages of a SOFC compared to most other fuel cell technologies is the possibility to use hydrocarbon fuels in addition to the more traditional hydrogen. However, the state-of-the-art SOFC with a Ni-based ceramic–metallic (cermet) anode is well-known to have some severe problems with hydrocarbon fuels, such as carbon build-up (coking) and sulfur poisoning, unless the fuel is desulfurized and reformed before use [1–3]. Thus there is a great interest to find alternative anode materials for SOFCs. Ceramic mixed ionic-electronic conductor (MIEC) materials have been identified as possible candidates to overcome many of the problems of the Ni-based anodes [2,3]. The Sr_2MgMoO_6 oxide with the *B*-site ordered $A_2B'B''O_6$-type double-perovskite structure is one of the most promising new ceramic anode materials. It has been found to yield high power densities when using methane as a fuel and to have good tolerance to sulphur [4,5]. Partial substitution of Sr^{II} by La^{III} was reported to further enhance the SOFC-anode performance of the phase for hydrocarbon fuels [6], but at the cost of lower stability under oxidizing conditions [7]. In addition to Sr_2MgMoO_6, other similar double perovskite molybdates, such as Sr_2MMoO_6 with M=Mn, Co or Ni, have also been tested as SOFC anodes [4,8]. In general, they have shown either lower performance or poorer stability than the M=Mg phase.

In this work we take a look at some practical issues concerning the synthesis of Sr_2MgMoO_6. We first study the reactions taking place during a typical solid-state synthesis with emphasis on the possible evaporation of molybdenum. The commonly used starting material MoO_3 has a low melting temperature of 795 °C and a high vapor pressure above this temperature [9]. It has therefore been questioned in the literature whether Mo will evaporate during the high-temperature synthesis of Sr_2MgMoO_6 [7,10]. By studying the reactions taking place between the commonly used starting materials, $SrCO_3$, $Sr(NO_3)_2$, MgO and MoO_3, we show that the evaporation of Mo during the solid-state synthesis of Sr_2MgMoO_6 is negligible due to the formation of $SrMoO_4$ at low temperatures.

Second, we consider some issues related to $SrMoO_4$ that is a common impurity in Sr_2MgMoO_6 samples [10–12] and in related Sr–Mo–O samples [13]. The $SrMoO_4$ compound with a scheelite structure and Mo at the oxidation state +VI is a white and insulating material [14]. It has therefore been proposed that $SrMoO_4$ could lower the electrical conductivity of the anode and increase the ohmic losses of the cell [7,15]. However, under reducing conditions $SrMoO_4$ tends to be reduced to the perovskite-structured $SrMoO_3$ with tetravalent Mo; this phase exhibits one of the highest electrical conductivities among oxide materials with a room temperature resistivity of ρ=5.1 μΩ cm measured for a single crystal [16–20]. To verify the effect of $SrMoO_4$ on the electrical conductivity of the anode, we prepared a series of Sr_2MgMoO_6 samples with different amounts of additional $SrMoO_4$.

* Corresponding author. Fax: +358 9 462 373.
E-mail address: maarit.karppinen@aalto.fi (M. Karppinen).

0022-4596/$ - see front matter © 2011 Elsevier Inc. All rights reserved.
doi:10.1016/j.jssc.2011.03.045

We show that under reducing conditions $SrMoO_4$ is reduced to $SrMoO_3$, which can in fact rather increase the electrical conductivity of the material.

2. Experimental

All the samples in this work were synthesized through solid-state reaction of stoichiometric mixtures of $SrCO_3$, MgO and MoO_3 powders. The MgO powder was calcined in air at 900 °C prior to use to decompose any traces of the hydrates and carbonates. The starting powder mixtures were first ground in a ball mill (Retsch Mixer Mill MM 400) for 60 minutes together with ethanol and then dried in an oven at 120 °C. The dried powder mixtures were calcined in air at 600–900 °C for 12 h, and then after regrinding in an agate mortar sintered either in air at 1200 or 1500 °C, or in 5% H_2/Ar at 1000 °C (see Section 3 for additional details). The sintering periods were 24 h long in all cases. For the series of Sr_2MgMoO_6 samples with additional $SrMoO_4$, the starting material composition corresponded to 0, 10, 20, 30, 40 and 50 wt% (or 0, 15, 28, 40, 51 and 61 mol%) of $SrMoO_4$. For these samples the calcination and sintering temperatures were 900 and 1200 °C, respectively, and the samples were pressed into pellets (20 mm in diameter and 1–2 mm in thickness) before sintering. It should be noted that the two phases, Sr_2MgMoO_6 and $SrMoO_4$, do not form solid solutions during the synthesis and can thus be synthesized together simply by changing the mole ratio of the starting materials.

The samples were examined by X-ray powder diffraction (XRD; PANanalytical X'Pert PRO MPD Alpha-1) with Cu $K\alpha_1$ radiation. To study the reactions taking place at the early stages of Sr_2MgMoO_6 synthesis, thermogravimetric (TG) studies of the typical starting materials, $SrCO_3$, $Sr(NO_3)_2$, MoO_3, and their mixtures of $SrCO_3$–MoO_3 and $Sr(NO_3)_2$–MoO_3 (Sr:Mo molar ratio of 1:1, mixed by grinding in an agate mortar) were performed with a heating rate of 5 °C/min in flowing air with a thermobalance (Perkin Elmer Pyris 1 TGA). The heating rate used was chosen to correspond roughly to the heating rates used in typical solid-state syntheses. The reducibility of the Sr_2MgMoO_6–$SrMoO_4$ samples was studied by TG in a 5% H_2/Ar gas flow with a heating rate of 2 °C/min. For all the TG measurements, powder specimens of 10–60 mg were heated up to a temperature of 1000 °C.

To detect any Mo losses during the high-temperature treatments of Sr_2MgMoO_6, we used inductively coupled plasma-atomic emission spectrometry (ICP-AES) to determine the Sr:Mo ratio for various samples from different stages of synthesis. Five samples were studied. Sample-1 was taken from a thoroughly ground mixture of the starting materials, $SrCO_3$, MgO and MoO_3. The rest of this mixture was calcined in air at 900 °C for 12 h and then thoroughly ground again. A part of this calcined powder was taken as a Sample-2. The remaining powder was divided into three parts and each was fired for 24 h under different conditions. One part was fired at 1000 °C in 5% H_2/Ar (Sample-3), another at 1200 °C in air (Sample-4) and the last at 1500 °C in air (Sample-5). These firing conditions were chosen as they represent the typical conditions of Sr_2MgMoO_6 synthesis (Samples 2, 3 and 4) or the highest temperature we could expose the material to (Sample-5). The samples were not pelletized in order to make them the "worst case scenarios", i.e. to allow for the greatest possible Mo evaporation. The ICP-AES measurements were performed with a Varian Liberty device. Three parallel measurements were carried out for each sample, and averages and standard deviations were calculated from the results. The initial ICP-AES results showed around 5% Mo excess for the samples (i.e. Sr:Mo ratio of 2:1.05 for Sample-1), but a similar Mo excess was also found for MoO_3 and $SrMoO_4$ used as reference samples. This Mo excess was therefore assumed to be caused by a systematic measurement error. For the purpose of this work, we scaled all the results such that Sample-1 had a Sr:Mo ratio of 2:1.00, as we were interested in changes in the Sr:Mo ratio, rather than the absolute values themselves.

Electrical conductivities of the Sr_2MgMoO_6–$SrMoO_4$ samples were measured in a 5% H_2/Ar gas flow with a conventional four-probe dc method. The sample powder was pressed into rectangular bars with the dimension of $10 \times 3 \times 1.5$ mm^3 and sintered in air at 1200 °C for 12 h. Electrical contacts were made with Pt wire and Pt paste. The resistances of the sample specimens were measured with a multimeter (Agilent 34401A). Before the conductivity measurement, the sample was first annealed in 5% H_2/Ar at 850 °C for 12 h to ensure that the samples were properly reduced. Temperature was then lowered to 500 °C and the measurement was started. The measurement was made at temperatures from 500 to 850 °C with an interval of 30–40 °C. The temperature was raised at a rate of 2 °C/min; but before each measurement, heating was stopped to allow the sample resistance to become stabilized.

3. Results and discussion

Results of the TG studies of $SrCO_3$, $Sr(NO_3)_2$, MoO_3 and the mixtures of $SrCO_3$–MoO_3 and $Sr(NO_3)_2$–MoO_3 are presented in Fig. 1. As can be seen, $SrCO_3$ starts to decompose to SrO at ~800 °C, but the decomposition remains incomplete even at 1000 °C at the heating rate used in this work. The other strontium precursor, $Sr(NO_3)_2$ begins to decompose already below 400 °C, but the decomposition proceeds through a step and the mass decreases more rapidly only above 550 °C. The weight change seen for $Sr(NO_3)_2$ is 52.5%, which is comparable to the expected weight-change value of 51.0% for the reaction of $Sr(NO_3)_2$ (s)→ SrO (s)+$2NO_x$ (g). The evaporation of MoO_3 starts already at ~650 °C, after which the sample mass quickly drops to zero (Fig. 1).

When MoO_3 is mixed with either $SrCO_3$ or $Sr(NO_3)_2$, the behavior of the samples during the heating changes notably (Fig. 1). In both cases the mass starts to decrease already below 400 °C, well below the evaporation temperature of MoO_3. The mass drops seen for $SrCO_3$–MoO_3 and $Sr(NO_3)_2$–MoO_3 are 15.1% and 30.2%, respectively. These values are in excellent agreement with the calculated weight changes of 15.1% and 30.4% for the reactions, $SrCO_3$ (s)+MoO_3 (s)→$SrMoO_4$ (s)+CO_2 (g) and $Sr(NO_3)_2$ (s)+MoO_3 (s)→$SrMoO_4$ (s)+$2NO_x$ (g), respectively. The XRD patterns (not shown here) revealed that in both cases the end product after the TG measurements was $SrMoO_4$ with no

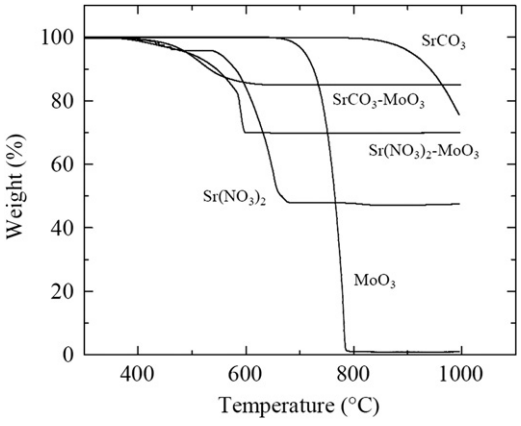

Fig. 1. TG curves for $SrCO_3$, $Sr(NO_3)_2$, MoO_3 and mixtures of $SrCO_3$–MoO_3 and $Sr(NO_3)_2$–MoO_3 recorded in air with a heating rate of 5 °C/min.

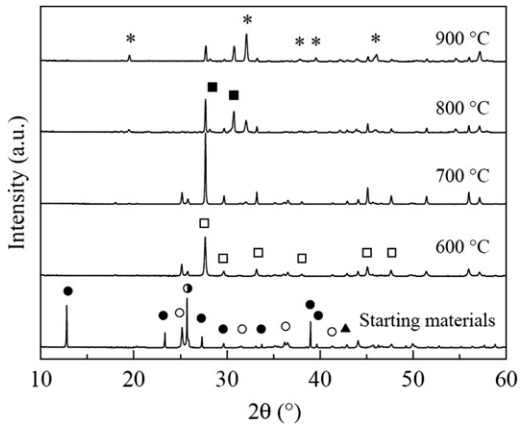

Fig. 2. XRD patterns for a mixture of $SrCO_3$, MgO and MoO_3 and the same sample after calcination at 600, 700, 800 or 900 °C for 12 h. The marked phases are $SrCO_3$ (○), MoO_3 (●), MgO (▲), $SrMoO_4$ (□), Sr_3MoO_6 (■) and Sr_2MgMoO_6 (*).

other phases. As can be seen from Fig. 1, both of the reactions are complete before the temperature required for the evaporation of MoO_3 is reached, and there is no sign of additional mass changes at temperatures up to 1000 °C in either of the samples after the formation of $SrMoO_4$. These results demonstrate that at the typical heating rates used in solid-state synthesis, $SrMoO_4$ is formed well before the evaporation of MoO_3 begins and that the $SrMoO_4$ phase is stable and can thus prevent the evaporation of molybdenum. At much higher heating rates, the formation of $SrMoO_4$ might not reach completion before the evaporation of MoO_3 starts, but we have not verified this experimentally. It should also be noted that in the case of Sr_2MgMoO_6 synthesis, the starting mixture contains twice as much $SrCO_3$ as MoO_3, which should further help to prevent molybdenum from escaping.

In order to verify the reactions taking place during the synthesis of Sr_2MgMoO_6, we recorded XRD patterns for a stoichiometric mixture of the starting materials, $SrCO_3$, MgO and MoO_3, and also for the same sample after calcination at 600, 700, 800 or 900 °C for 12 h. The results are presented in Fig. 2. After firing at 600 °C, below the temperature required for MoO_3 evaporation, the XRD data reveal that all of the MoO_3 has reacted to form $SrMoO_4$, as is expected based on the TG results. The MgO and some of the $SrCO_3$ are still left unreacted at this temperature. The data for the sample fired at 700 °C show that a tiny amount of Sr_2MgMoO_6 is already formed at this relatively low temperature, but otherwise there is no appreciable difference compared to the sample calcined at 600 °C, except for the improved crystallization of $SrMoO_4$. In the sample calcined at 800 °C, $SrCO_3$ has almost completely disappeared, the amount of $SrMoO_4$ has decreased compared to the sample fired at 700 °C, and a notable amount of Sr_3MoO_6 has been formed by a reaction between $SrMoO_4$ and $SrCO_3$. There is also more Sr_2MgMoO_6 formed compared to the sample fired at 700 °C. After firing at 900 °C, even more Sr_2MgMoO_6 has been formed while the amounts of $SrMoO_4$, Sr_3MoO_6 and MgO have slightly decreased. These results are very similar to those reported previously by Marrero-López et al. [10].

The aforementioned results strongly suggest that during the solid-state synthesis of Sr_2MgMoO_6, $SrCO_3$ and MoO_3 first react to form $SrMoO_4$ at low temperatures, as shown by the TG results, and the formation of Sr_2MgMoO_6 then goes through reactions between the $SrMoO_4$ and the yet remaining $SrCO_3$ and MgO. The formation of a small amount of Sr_2MgMoO_6 and the absence of Sr_3MoO_6 in the sample fired at 700 °C illustrate that the reactivities of $SrCO_3$ and MgO with $SrMoO_4$ are at similar levels at this temperature. On the other hand, the formation of Sr_3MoO_6 in the sample calcined at 800 °C indicates that the increased temperature increases the reactivity of $SrCO_3$ compared to that of MgO. This results in the formation of Sr_3MoO_6, as not enough MgO can react to form Sr_2MgMoO_6. It is therefore evident that at higher temperatures the rate of diffusion of MgO is the limiting factor in the synthesis of Sr_2MgMoO_6. Using more reactive starting materials for magnesium, such as $MgCO_3$, might allow for better reactivity of the starting materials and thereby lowering of the synthesis temperature.

The results so far have shown that the evaporation of molybdenum at temperatures up to 1000 °C is effectively hindered by the formation of $SrMoO_4$ at low temperatures. However, it might still be possible for molybdenum to escape during the long-lasting high-temperature sintering during the final stages of Sr_2MgMoO_6 synthesis. We therefore employed ICP-AES to detect any such molybdenum losses under typical Sr_2MgMoO_6 sintering conditions. The resultant Sr:Mo ratios for the samples are presented in Table 1. The results show that when the firing temperature was increased up to 1200 °C, there was a small decrease in the amount of Mo compared to that of Sr; the maximum molybdenum losses detected were of the order of 1% in Samples 3 and 4. However, these changes are within the standard deviations of the measurements. Therefore, in the limits of detection, the loss of molybdenum in typical synthesis conditions up to the temperature of 1200 °C appears to be negligible.

Unlike Samples 2, 3 and 4, Sample-5, calcined at 900 °C and sintered at 1500 °C, shows an increase of ca. 2% in the relative amount of Mo, when compared to the starting material mixture (Table 1). We believe that this apparent increase is caused by partial decomposition of Sr_2MgMoO_6 and subsequent evaporation of strontium either as elemental Sr or as SrO. The boiling point of Sr is 1382 °C [9], and according to literature [21], SrO has a small but finite vapor pressure at 1500 °C and could thus evaporate when being freely available in the sample. Our XRD data (not shown here) revealed that when phase-pure Sr_2MgMoO_6 samples, prepared at 1200 °C, were subsequently fired at 1500 °C, increased amounts of $SrMoO_4$ and MgO were formed. This result would indicate that at the high temperature of 1500 °C, Sr_2MgMoO_6 partially decomposes to $SrMoO_4$, MgO, and most probably to SrO that, however, appears at least partially to evaporate. It should be noted that MgO has also a finite vapor pressure at 1500 °C [21], which could cause some of it to evaporate, but we did not verify this. Typically, there is no need for such high temperatures in synthesizing Sr_2MgMoO_6, so considering the SOFC applications, the high temperature decomposition should not be an issue.

Concerning the decomposition of Sr_2MgMoO_6, Marrero-López et al. [15] found that samples synthesized under reducing conditions degraded in a matter of days when stored in air, even at room temperature. We have noticed similar signs of degradation in our samples synthesized under reducing conditions, but not in samples synthesized in air. Fig. 3 shows a close-up of the XRD patterns for an as-synthesized Sr_2MgMoO_6 sample (see also Fig. 4), synthesized in air at 1200 °C with the solid-state method described in this work and of the same sample after storing in air

Table 1
ICP-AES data for the Sr:Mo ratio in the starting material powder mixture and in the same powder mixture after various heat treatments.

Sample	Description	Sr:Mo
1	Powder mixture: $2SrCO_3+MgO+MoO_3$	2:1.00(1)
2	Same mixture after firing: 900 °C, 12 h, air	2:0.998(5)
3	900 °C, 12 h, air+1000 °C, 24 h, H_2/Ar	2:0.992(8)
4	900 °C, 12 h, air+1200 °C, 24 h, air	2:0.991(9)
5	900 °C, 12 h, air+1500 °C, 24 h, air	2:1.019(3)

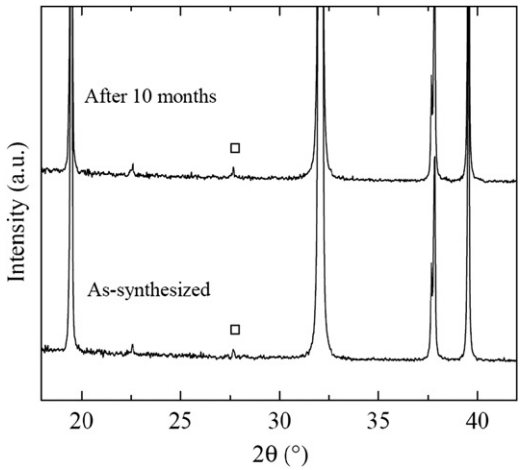

Fig. 3. Close-up of the XRD patterns for an as-synthesized Sr_2MgMoO_6 sample synthesized in air at 1200 °C, and for the same sample after storing in air for 10 months. The impurity phase $SrMoO_4$ is marked with open squares (□).

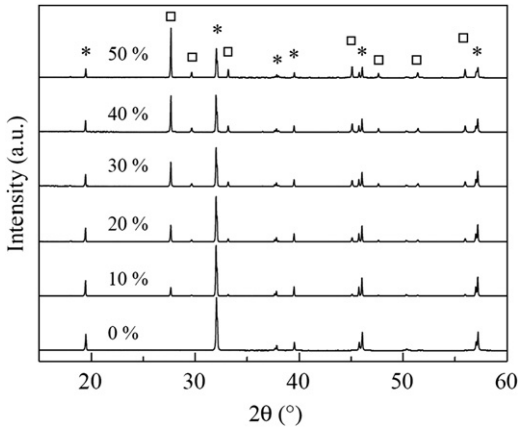

Fig. 4. XRD patterns for the Sr_2MgMoO_6 samples with 0, 10, 20, 30, 40 and 50 wt% of $SrMoO_4$. The major reflections of $SrMoO_4$ (□) and Sr_2MgMoO_6 (*) are marked.

for 10 months. The as-synthesized sample contained a tiny amount of $SrMoO_4$, but the amount did not increase during the storage, nor were there signs of any new phases. These results show that Sr_2MgMoO_6 samples synthesized in air are more stable than those synthesized under reductive conditions. This finding is reasonable as the samples synthesized under reductive conditions have a more disordered structure (lower degree of *B*-site cation order), more oxygen vacancies, and Mo in a lower valence state than in case of the samples sintered in air [11,15], and are thus expected to be more unstable and more reactive. However, the very same properties give the more reduced material the higher electrical conductivity [10,15] and presumably also better performance as an SOFC anode compared to the samples synthesized in air. Therefore, there seems to be a balance between the long-term stability of Sr_2MgMoO_6 and its performance as an anode. Additional study of the materials stability would be needed to determine, for example, if the air-synthesized samples degrade after they have been reduced. In addition, the possible formation of metal carbonates on the materials surface under carbon-containing atmosphere, as discussed by Marrero-López et al. [15], could be a problem even for Sr_2MgMoO_6 samples synthesized in air.

As we have shown in this work, $SrMoO_4$ is a stable compound, forming in the early stage of Sr_2MgMoO_6 synthesis; it has therefore been found in many previous studies as a common impurity phase. As was discussed in Section 1, $SrMoO_4$ is insulating, but is relatively easily reduced to $SrMoO_3$, which is highly conductive. We therefore prepared a series of Sr_2MgMoO_6 samples with 0, 10, 20, 30, 40 and 50 wt% of $SrMoO_4$ in order to study how the $SrMoO_4$ addition affects the material's electrical properties under reducing conditions. Fig. 4 shows XRD patterns for the Sr_2MgMoO_6–$SrMoO_4$ sample series. Almost completely phase-pure Sr_2MgMoO_6 was obtained in this study from the stoichiometric starting material mixture (see Fig. 3 for the close-up of the Sr_2MgMoO_6 sample), which we attribute to the proper mixing and possible activation of the starting materials by intensive ball milling. In addition to Sr_2MgMoO_6 and $SrMoO_4$, no other phases were detected in any of the Sr_2MgMoO_6–$SrMoO_4$ samples.

Under reducing conditions, $SrMoO_4$ in the mixtures is reduced to $SrMoO_3$. This can be seen in the TG curve (shown in Fig. 5) recorded for the reduction (in 5% H_2/Ar) of a Sr_2MgMoO_6–$SrMoO_4$ sample with 50 wt% of $SrMoO_4$. The mass starts to decrease at ~750 °C, and the measured mass drop of 3.3% is in excellent agreement with the value of 3.2%, calculated assuming that $SrMoO_4$ is completely reduced to $SrMoO_3$. The Sr_2MgMoO_6 phase itself should also get slightly reduced, but it is not clearly noticeable in this mass-change range. Fig. 6 shows, as an example, the XRD patterns for the Sr_2MgMoO_6–$SrMoO_4$ system with 20 wt% of $SrMoO_4$ after synthesis in air and for the same sample after reduction in 5% H_2/Ar at 850 °C for 12 h. It can be seen that $SrMoO_4$ in the as-synthesized sample has been completely

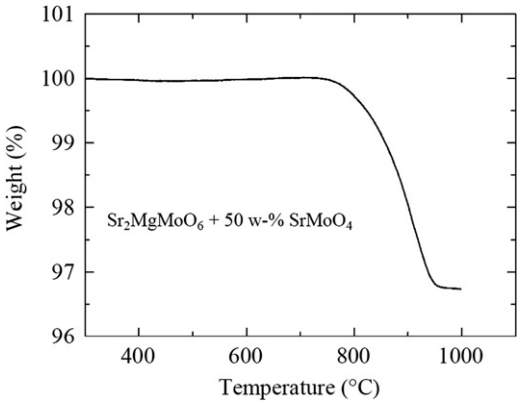

Fig. 5. TG curve for the Sr_2MgMoO_6 sample with 50 wt% of $SrMoO_4$ reduced in 5% H_2/Ar with a heating rate of 2 °C/min.

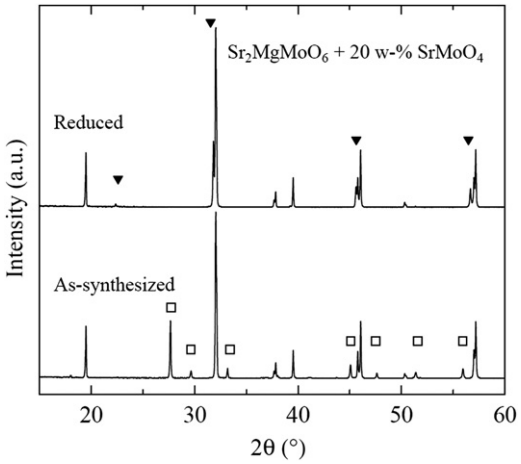

Fig. 6. XRD patterns of the as-synthesized Sr_2MgMoO_6 samples 20 w-% of $SrMoO_4$ and of the same sample after reduction. Major reflections of $SrMoO_4$ (□) and $SrMoO_3$ (▼) are marked, and the unmarked peaks are due to Sr_2MgMoO_6.

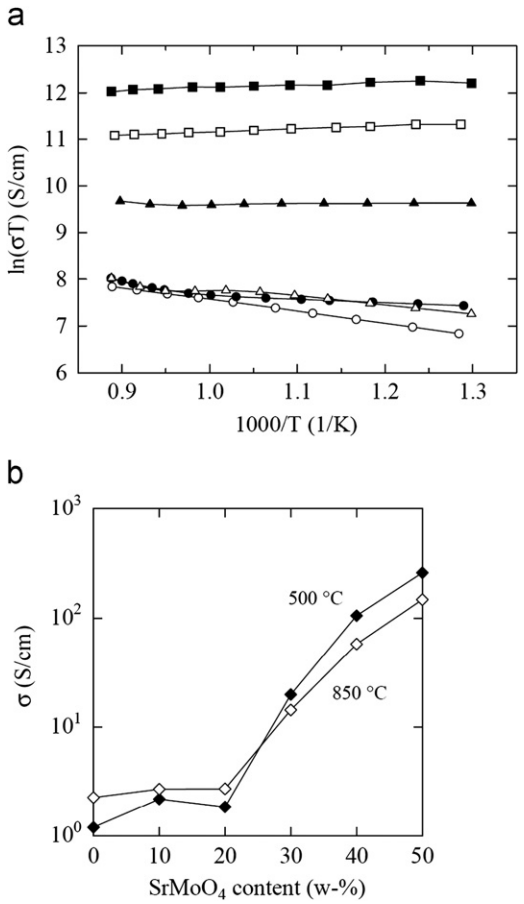

Fig. 7. (a) Electrical conductivities for the Sr_2MgMoO_6 samples with 0 (○), 10 (●), 20 (Δ), 30 (▲), 40 (□) and 50 wt% (■) of $SrMoO_4$ as a function of temperature. (b) Electrical conductivities of the Sr_2MgMoO_6–$SrMoO_4$ samples as a function of $SrMoO_4$ content in (◆) 500 °C and (◇) 800 °C. The measurements were done in 5% H_2/Ar.

reduced to $SrMoO_3$ with no sign of other phases. The same behavior was observed for all the other samples.

Fig. 7(a) and (b) shows the electrical conductivities of the Sr_2MgMoO_6–$SrMoO_4$ samples with varying amounts of $SrMoO_4$. Pure Sr_2MgMoO_6 shows a linear behavior in the Arrhenius-plot, as has been found in our previous study [12], with electrical conductivity of ca. 2 S/cm at 800 °C. With $SrMoO_4$ contents of 10–20 wt%, the conductivity changes only slightly, although there is a clear deviation from the linear behavior at lower temperatures, where the conductivities are somewhat higher than that of Sr_2MgMoO_6. For 30 wt% of $SrMoO_4$ or more, the conductivity of the sample increases noticeably. The conductivity values at 800 °C were 14, 60 and 160 S/cm for the samples with 30, 40 and 50 wt% of $SrMoO_4$, respectively. As Fig. 7(a) and (b) shows the conductivity also changes to metallic type with increasing amount of $SrMoO_4$ (or $SrMoO_3$). The sudden increase of conductivity at 20–30 wt% of $SrMoO_4$ is clearly caused by percolation of the $SrMoO_4$ (or $SrMoO_3$) particles in the Sr_2MgMoO_6 matrix. As percolation is related to the volume fractions of the phases, rather than their weight fractions, we calculated the volume percentages of the different phases in the samples. The theoretical densities of Sr_2MgMoO_6, $SrMoO_4$ and $SrMoO_3$ (calculated using the unit cell volumes [12,14,20] and molar masses of the materials) are 5.28, 4.74 and 6.12 g/cm^3, respectively. The similar magnitude of the densities means that the volume percentages are rather close to the weight percentages. In case of the as-synthesized samples with $SrMoO_4$ mixed with Sr_2MgMoO_6, the weight percentages of 10, 20, 30, 40, 50 w% correspond to 11, 22, 32, 43, 53 V%, respectively. When $SrMoO_4$ is reduced to $SrMoO_3$, the density increases and the corresponding volume percentages are 8, 17, 26, 35 and 45 V%. Thus it can be concluded that the increase in electrical conductivity due to the percolation of $SrMoO_3$ particles in Sr_2MgMoO_6 matrix takes place when the volume fraction of $SrMoO_3$ is between 17% and 26%.

It should be noted here that the electrical conductivities had some sample-to-sample variation. For example, one preliminary test sample with 35 wt% of $SrMoO_4$ had a higher conductivity than the sample with 40 wt% of $SrMoO_4$ discussed here. This is assumed to be due to differences in the exact microstructure of the samples, such as the size and distribution of the $SrMoO_4$ particles, a phenomenon which is well known for the traditional Ni-based cermet anodes and ceramic composite cathodes [1].

$SrMoO_3$ and $SrMoO_4$ have been found to have some catalytic activity for hydrocarbon oxidation [19], which could be advantageous in SOFC anode use. However, one notable source of possible problems in using $SrMoO_4$ as an SOFC anode component is the fact that the unit-cell volume per formula unit of $SrMoO_4$ decreases by 28% upon the reduction of the phase to $SrMoO_3$ (calculated using the structural data from Refs. 14 and 20). Such a large volume change could cause the anode to detach from the electrolyte during redox cycling. During our conductivity tests of the Sr_2MgMoO_6–$SrMoO_4$ sample series, we saw no cracks in the pellets or other indications of mechanical problems caused by the reduction of $SrMoO_4$ even after repeated reductions and oxidations. However, the situation of a single dense pellet is quite different from that of the actual fuel cell set-up with a porous anode sintered to the surface of an electrolyte. While $SrMoO_4$ in itself is not expected to be dimensionally stable enough to work as an SOFC anode, it is possible that the Sr_2MgMoO_6–$SrMoO_4$ composites function similarly to the Ni-cermets, in which NiO is mixed with the electrolyte material and later reduced, forming a porous electrolyte scaffolding holding the Ni-particles [1]. Theoretically, the bulk volume of NiO is reduced by 40.9% upon reduction to Ni [22], i.e. even more than in the case of $SrMoO_4$. In the same way Sr_2MgMoO_6 could work as the scaffolding holding the $SrMoO_4$ particles, as long as the amount of $SrMoO_4$ is low enough. Proper cell tests would naturally be needed to determine whether the Sr_2MgMoO_6–$SrMoO_4$ composites show any improvement in the SOFC performance and what are the effects of the $SrMoO_4$ volume change on the long-term stability of the anode.

4. Conclusions

In this work we have shown that evaporation of molybdenum during a typical solid-state synthesis of Sr_2MgMoO_6 is negligible due to the formation of $SrMoO_4$ at low temperatures. However, at the high temperature of 1500 °C Sr_2MgMoO_6 was found to partially decompose; but as there is no need for such high temperatures in synthesizing Sr_2MgMoO_6, the decomposition should not be an issue. In addition, we found that Sr_2MgMoO_6 synthesized in air appears to be more stable than when synthesized under reductive conditions.

The $SrMoO_4$ formed during the synthesis has been assumed to be detrimental to the electrical properties of Sr_2MgMoO_6, but we showed that under reducing conditions $SrMoO_4$ is reduced to $SrMoO_3$, which actually increases the materials electrical conductivity. Normally signs of $SrMoO_4$ would indicate incomplete reactions during the synthesis, and there should then also be SrO (or $SrCO_3$) and MgO left unreacted, which are expected to lower the materials electrical conductivity, whereas $SrMoO_4$ is not.

Due to its reduction to $SrMoO_3$ having a high electrical conductivity, $SrMoO_4$ could be used as an SOFC anode component. However, the unit cell volume of $SrMoO_4$ is greatly decreased during reduction, which is unacceptable for an SOFC anode. A composite of Sr_2MgMoO_6 and $SrMoO_4$ could have better dimensional stability, at least as long as the amount of $SrMoO_4$ is low enough. Therefore, the Sr_2MgMoO_6–$SrMoO_4$ composite demonstrates the possibility of using more than one ceramic material to perform different tasks in the anode, similar to the traditional Ni-cermet anodes or the ceramic composite cathodes. This basic principle is applicable to other ceramics as well, but the Sr_2MgMoO_6–$SrMoO_4$ system is interesting because Sr_2MgMoO_6 is in itself a good anode material, and $SrMoO_4$, when reduced to $SrMoO_3$, has a very high electrical conductivity. In addition, Sr_2MgMoO_6 and $SrMoO_4$ can be synthesized together, which would simplify the processing.

Acknowledgments

The authors thank Prof. J.B. Goodenough for fruitful discussions. The present work was supported by Academy of Finland (Nos. 126528 and 116254) and Tekes (No. 1726/31/07).

References

[1] S.C. Singhal, K. Kendall, High-temperature Solid Oxide Fuel Cells: Fundamentals, Design and Applications, Elsevier Science, New York, 2003.
[2] C. Sun, U.J. Stimming, J. Power Sources 171 (2007) 247.
[3] J.B. Goodenough, Y.H. Huang, J. Power Sources 173 (2007) 1.
[4] Y.H. Huang, R.I. Dass, Z.L. Xing, J.B. Goodenough, Science 312 (2006) 254–257.
[5] Y.H. Huang, R.I. Dass, J.C. Denyszyn, J.B. Goodenough, J. Electrochem. Soc. 153 (2006) A1266–A1272.
[6] Y. Ji, Y.H. Huang, J.R. Ying, J.B. Goodenough, Electrochem. Commun. 9 (2007) 1881–1885.
[7] D. Marrero-López, J. Peña-Martínez, J.C. Ruiz-Morales, M.C. Martín-Sedeño, P.J. Núñez, Solid State Chem 182 (2009) 1027–1034.
[8] Y.H. Huang, G. Liang, M. Croft, M. Lehtimäki, M. Karppinen, J.B. Goodenough, Chem. Mater. 21 (2009) 2319–2326.
[9] R.C. Weast, CRC Handbook of Chemistry and Physics, 69th Edition, CRC Press, Boca Raton, 1989.
[10] D. Marrero-López, J. Penã-Martínez, J.C. Ruiz-Morales, D. Pérez-Coll, M.A.G. Aranda, P. Núñez, Mater. Res. Bull. 43 (2008) 2441–2450.
[11] C. Bernuy-Lopez, M. Allix, C.A. Bridges, J.B. Claridge, M.J. Rosseinsky, Chem. Mater. 19 (2007) 1035–1043.
[12] S. Vasala, M. Lehtimäki, S.C. Haw, J.M. Chen, R.S. Liu, H. Yamauchi, M. Karppinen, Solid State Ionics 181 (2010) 754–759.
[13] S. Vasala, M. Lehtimäki, Y.H. Huang, H. Yamauchi, J.B. Goodenough, M. Karppinen, J. Solid State Chem. 183 (2010) 1007–1012.
[14] J.C. Sczancoski, L.S. Cavalcante, M.R. Joya, J.A. Varela, P.S. Pizani, E. Longo, Chem. Eng. J. 140 (2008) 632–637.
[15] D. Marrero-López, J. Peña-Martínez, J.C. Ruiz-Morales, M. Gabás, P. Núñez, M.A.G. Aranda, J.R. Ramos-Barrado, Solid State Ionics 180 (2010) 1672–1682.
[16] I. Nagai, N. Shirakawa, S.I. Ikeda, R. Iwasaki, H. Nishimura, M. Kosaka, Appl. Phys. Lett. 87 (2005) 024105-1–024105-3.
[17] T. Maekawa, K. Kurosaki, H. Muta, M. Uno, S. Yamanaka, J. Alloy Compd. 390 (2005) 314–317.
[18] D. Logvinovich, R. Aguiar, R. Robert, M. Trottmann, S.G. Ebbinghaus, A. Reller, A. Weidenkaff, J. Solid State Chem. 180 (2007) 2649–2654.
[19] J. Kubo, W. Ueda, Mater. Res. Bull. 44 (2009) 906–912.
[20] R.B. Macquart, B.J. Kennedy, M. Avdeev, J. Solid State Chem. 183 (2010) 249–254.
[21] R.H. Lamoreaux, D.L. Hildenbrand, L. Brewer, J. Phys. Chem. Ref. Data 16 (1987) 419–443.
[22] D. Waldbillig, A. Wood, D.G. Ivey, Solid State Ionics 176 (2005) 847–859.